(*23*) and speculate that even higher-order processes should become accessible when one eliminates residual parabolic energy shifts due to the trapping laser beams.

Our results underline the utility of cold atoms in optical lattices for the investigation of fundamental physical processes driven by small-amplitude terms and specifically higher-order tunneling. By partly freezing the motion in the deep lattice, these sensitive processes can be observed here despite finite initial temperatures (which here are converted into defects and missing atoms in an ensemble of initial states). This will motivate further investigation of quantum phases and critical properties near these higher-order resonances, which are presently unknown, including systems with tilts along multiple axes (*19*, *30*). Our initial studies of parameter reversals also open the door to the study of many-body dephasing and echo-type experiments on a quantum many-body system, as well as investigations into the nature of the many-body dephasing and (apparent) thermalization (*31*). Parallels can be drawn with arrays of quantum dots, opening further possibilities to model electron tunneling over multiple sites (*11*) by using fermionic atoms.

REFERENCES AND NOTES

1. J. Ankerhold, *Quantum Tunneling in Complex Systems: The Semiclassical Approach* (Springer, Berlin, 2010).
2. O. Morsch, M. Oberthaler, *Rev. Mod. Phys.* **78**, 179–215 (2006).
3. A. H. MacDonald, S. M. Girvin, D. Yoshioka, *Phys. Rev. B* **37**, 9753–9756 (1988).
4. P. W. Anderson *et al.*, *J. Phys. Condens. Matter* **16**, R755–R769 (2004).
5. M. R. Norman, *Science* **332**, 196–200 (2011).
6. R. Ma *et al.*, *Phys. Rev. Lett.* **107**, 095301 (2011).
7. S. Fölling *et al.*, *Nature* **448**, 1029–1032 (2007).
8. S. Trotzky *et al.*, *Science* **319**, 295–299 (2008).
9. D. Greif, T. Uehlinger, G. Jotzu, L. Tarruell, T. Esslinger, *Science* **340**, 1307–1310 (2013).
10. E. Dagotto, *Rev. Mod. Phys.* **66**, 763–840 (1994).
11. F. R. Braakman, P. Barthelemy, C. Reichl, W. Wegscheider, L. M. K. Vandersypen, *Nat. Nanotechnol.* **8**, 432–437 (2013).
12. S. Sachdev, *Nat. Phys.* **4**, 173–185 (2008).
13. F. Queisser, P. Navez, R. Schützhold, *Phys. Rev. A* **85**, 033625 (2012).
14. G. Sedghi *et al.*, *Nat. Nanotechnol.* **6**, 517–523 (2011).
15. J. R. Winkler, H. B. Gray, *J. Am. Chem. Soc.* **136**, 2930–2939 (2014).
16. C. Sias *et al.*, *Phys. Rev. Lett.* **98**, 120403 (2007).
17. J. Simon *et al.*, *Nature* **472**, 307–312 (2011).
18. W. S. Bakr *et al.*, *Nature* **480**, 500–503 (2011).
19. S. Sachdev, K. Sengupta, S. M. Girvin, *Phys. Rev. B* **66**, 075128 (2002).
20. F. Meinert *et al.*, *Phys. Rev. Lett.* **111**, 053003 (2013).
21. M. Kolodrubetz, D. Pekker, B. K. Clark, K. Sengupta, *Phys. Rev. B* **85**, 100505 (2012).
22. D. Jaksch, C. Bruder, J. I. Cirac, C. W. Gardiner, P. Zoller, *Phys. Rev. Lett.* **81**, 3108–3111 (1998).
23. Materials, methods, and additional theoretical background are available as supporting material on *Science* Online.
24. L. Amico, R. Fazio, A. Osterloh, V. Vedral, *Rev. Mod. Phys.* **80**, 517–576 (2008).
25. S. Trotzky *et al.*, *Nat. Phys.* **8**, 325–330 (2012).
26. C. Kollath, A. M. Läuchli, E. Altman, *Phys. Rev. Lett.* **98**, 180601 (2007).
27. T. Weber, J. Herbig, M. Mark, H.-C. Nägerl, R. Grimm, *Science* **299**, 232–235 (2003).
28. The lattice depth V_q is calibrated by Kapitza-Dirac diffraction. The statistical error for V_q is 1%, although the systematic error can reach up to 5%. We give all energies in frequency units.
29. H. Lignier *et al.*, . *Phys. Rev. Lett.* **99**, 220403 (2007).
30. S. Pielawa, T. Kitagawa, E. Berg, S. Sachdev, *Phys. Rev. B* **83**, 205135 (2011).
31. M. Rigol, V. Dunjko, M. Olshanii, *Nature* **452**, 854–858 (2008).
32. The matter-wave interference pattern is fit by $n(p) = N_0 e^{-(p-p_0)^2/w^2}(1 + V\cos[k(p-p_0) + \phi])$ with the fringe visibility V, the wave vector k, and a phase ϕ.

ACKNOWLEDGMENTS

We are indebted to R. Grimm for generous support and thank J. Schachenmayer for discussions and contributions to numerical code development. We gratefully acknowledge funding by the European Research Council (ERC) under project no. 278417 and support in Pittsburgh from NSF grant PHY-1148957.

SUPPLEMENTARY MATERIALS

www.sciencemag.org/content/344/6189/1259/suppl/DC1
Supplementary Text
Figs. S1 to S5
References (*33*–*37*)

11 November 2013; accepted 19 May 2014
10.1126/science.1248402

QUANTUM MECHANICS

Mechanically detecting and avoiding the quantum fluctuations of a microwave field

J. Suh,[1,2] A. J. Weinstein,[1,2] C. U. Lei,[1,2] E. E. Wollman,[1,2] S. K. Steinke,[1,3] P. Meystre,[3] A. A. Clerk,[4] K. C. Schwab[1,2]*

Quantum fluctuations of the light field used for continuous position detection produce stochastic back-action forces and ultimately limit the sensitivity. To overcome this limit, the back-action forces can be avoided by giving up complete knowledge of the motion, and these types of measurements are called "back-action evading" or "quantum nondemolition" detection. We present continuous two-tone back-action evading measurements with a superconducting electromechanical device, realizing three long-standing goals: detection of back-action forces due to the quantum noise of a microwave field, reduction of this quantum back-action noise by 8.5 ± 0.4 decibels (dB), and measurement imprecision of a single quadrature of motion 2.4 ± 0.7 dB below the mechanical zero-point fluctuations. Measurements of this type will find utility in ultrasensitive measurements of weak forces and nonclassical states of motion.

During the theoretical investigation of the ultimate sensitivity of gravitational wave detectors in the 1970s, it was understood how quantum physics places limits on measurements of motion (*1*, *2*). For continuous position measurements, the quantum back-action forces from vacuum fluctuations of the detection light field limit the sensitivity at the standard quantum limit (SQL) (*2*). Recently, the detection of motion has advanced to the point that quantum back-action engineering has become necessary to improve measurement sensitivity. Position imprecision below the SQL has been achieved in microwave (*3*) and optical (*4*) systems, force sensitivity near the quantum limit has been demonstrated with cold atoms (*5*), and quantum back-action forces from electronic currents (*6*) or optical fields (*7*, *8*) have been observed. The quantum back-action can be manipulated by modulating the coupling between the detection field and mechanical element, where the coupling modulation can be implemented by either sudden stroboscopic measurement (*9*, *10*) or continuous two-tone back-action evading (BAE) measurement (*11*–*14*).

Our system is a microwave-frequency parametric transducer of motion (Fig. 1A): A mechanical resonator ($\omega_m = 2\pi \times 4.0074$ MHz) modulates the capacitance of a superconducting electrical resonator ($\omega_c = 2\pi \times 5.4481$ GHz), and modifies ω_c by 13.8 ± 0.3 Hz ($g_0/2\pi$) per x_{zp}, where $x_{zp} = \sqrt{\hbar/(2m\omega_m)} \approx 1.8$ fm is the amplitude of zero-point fluctuations of the mechanical resonator with mass m (*15*–*17*). The intrinsic damping rate of the mechanical resonator is $\Gamma_{m0} = 2\pi \times 10$ Hz at 20 mK. The damping rate of the electrical resonator is $\kappa = 2\pi(869 \pm 9)$ kHz, which places this system into the sideband resolved limit ($\omega_m > \kappa$) required to realize BAE dynamics (*14*, *18*). The excitation and read-out of the electrical resonator is achieved via input and output ports, with coupling rates of $\kappa_L = 2\pi(0.15 \pm 0.04)$ MHz and $\kappa_R = 2\pi(0.5 \pm 0.1)$ MHz, respectively.

We investigate the device by monitoring the response when driven by a carefully engineered microwave field (Fig. 1B). When driving the device with a coherent microwave tone ("pump") at $\omega_p = \omega_c - \omega_m$, the electromechanical coupling together with mechanical motion results in frequency up-conversion of pump photons to ω_c in a Raman-like process at a rate $n_m\Gamma_{opt}$, where n_m is the occupation factor of the mechanical mode, and $\Gamma_{opt} = 4g_0^2 n_p/\kappa$, with n_p as the number of

[1]Applied Physics, California Institute of Technology, Pasadena, CA 91125, USA. [2]Kavli Nanoscience Institute, California Institute of Technology, Pasadena, CA 91125, USA. [3]Department of Physics, University of Arizona, Tucson, AZ 85721, USA. [4]Department of Physics, McGill University, Montreal, Quebec, H3A 2T8 Canada.
*Corresponding author. E-mail: schwab@caltech.edu

pump photons in the electrical resonator. Similarly, when driving at $\omega_p = \omega_c + \omega_m$, photons are down-converted at a rate $(n_m+1)\Gamma_{opt}$ (*19*). These up- or down-converted sidebands are the signals analyzed; examples of the measured power spectra of these sidebands are shown in Fig. 3.

The sideband powers are calibrated by measuring the thermomechanical fluctuations at calibrated sample temperatures (*20*, *21*) (Fig. 1C). During the thermal calibration, we observe that the thermalization of the weakly pumped device at ultralow temperature is excellent, evidenced by the motional sideband corresponding to 7.2 ± 0.2 mK at the base temperature of our refrigerator (Fig. 1C, red cross and inset). Also, with a back-action damping measurement (*19*, *21*, *22*), we calibrate n_p (Fig. 1D). In all the following measurements, we feedback-control the sample temperature at 20.0 ± 0.2 mK with our calibrated RuO resistance thermometer to ensure an accurate and stable thermal environment.

In this system, two-tone BAE is accomplished by modulating the microwave pump field in the resonator: $a_{pump}(t) = \sqrt{2n_p}\cos\omega_m t \cdot \cos\omega_c t = \sqrt{n_p/2}[\cos(\omega_c - \omega_m)t + \cos(\omega_c + \omega_m)t]$. The modulation has the effect of coupling to a single mechanical quadrature, X_1, where $x(t) = X_1(t)\cos\omega_m t + X_2(t)\sin\omega_m t$. The BAE nature can be understood by noting that the back-action force produced at the mechanical frequency by the beating between voltage noise at the microwave resonance and the large pump field produces displacements exclusively in the X_2 quadrature (*18*). In this way, one gains information about X_1 and places both the classical and quantum back-action into X_2. Here, the classical back-action is due to thermal and technical noise in the microwave field, quantified by the effective occupation factor n_c. In contrast, the quantum back-action is due to the vacuum fluctuations of the electromagnetic field when the electrical resonator is in the quantum ground state ($n_c = 0$). This back-action

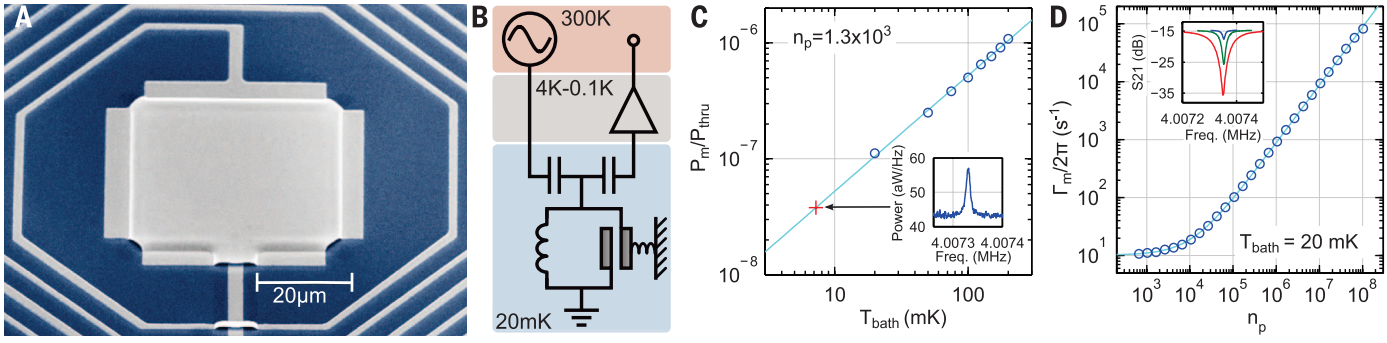

Fig. 1. Device, measurement scheme, and sample characterization. (**A**) Device electron micrograph. A parallel plate capacitor is connected to a spiral inductor, forming a lumped-element microwave resonator. The top plate of the capacitor is a compliant membrane, and we study its fundamental mechanical resonance (blue, silicon; gray, aluminum). (**B**) Measurement scheme. Shot-noise-limited microwave tones are applied to the device, and the output microwave field from the device is amplified by a low-noise amplifier at 4.2 K for analysis (*21*). (**C**) Calibration of motional sidebands (blue circles and line). (Inset) Motional sideband at base temperature. (**D**) Back-action damping. In addition to a red-detuned pump, a weak probe sweeping near the electrical resonance is applied, and its absorption shows the resonant mechanical response. Blue circle, mechanical damping rate; blue line, back-action damping theory fit (*19*). (Inset) Examples of absorption spectra at $n_p \approx 5 \times 10^3$, 3×10^4, and 1×10^5 from top to bottom.

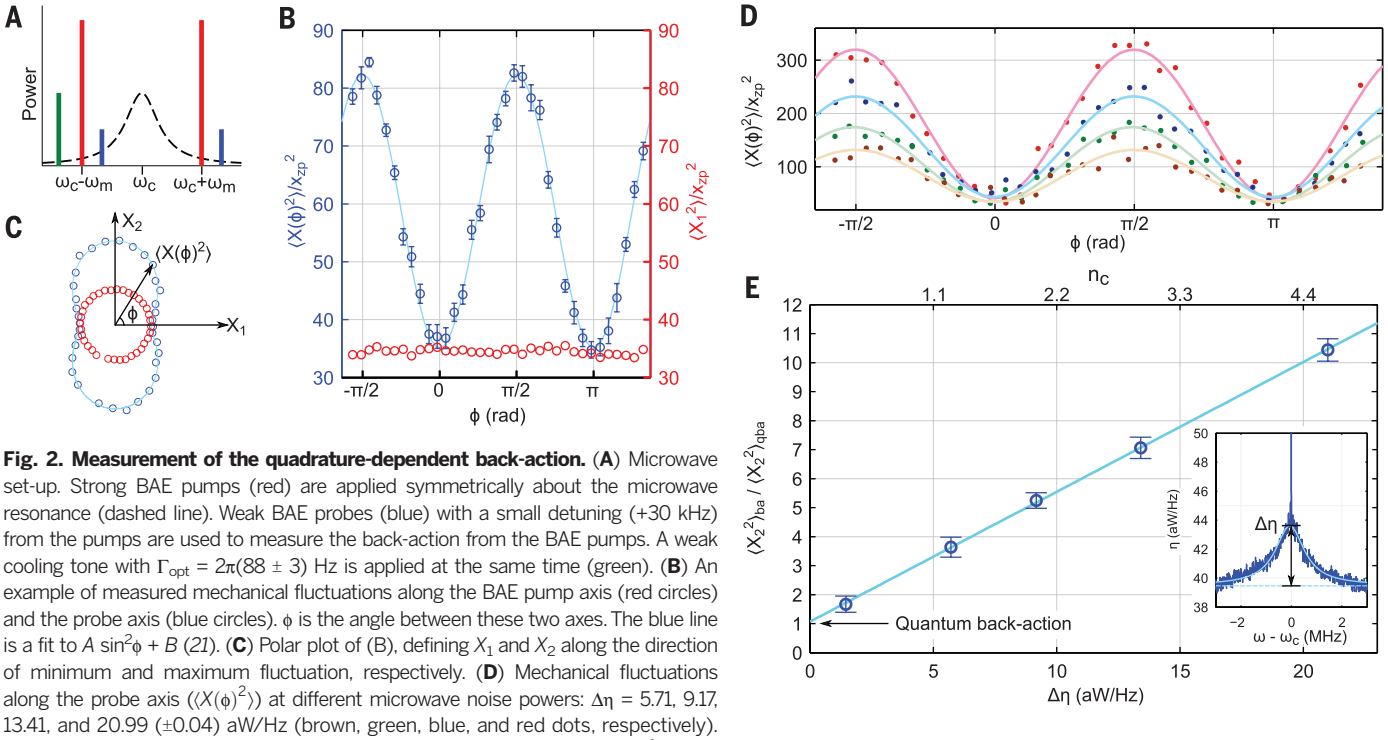

Fig. 2. Measurement of the quadrature-dependent back-action. (**A**) Microwave set-up. Strong BAE pumps (red) are applied symmetrically about the microwave resonance (dashed line). Weak BAE probes (blue) with a small detuning (+30 kHz) from the pumps are used to measure the back-action from the BAE pumps. A weak cooling tone with $\Gamma_{opt} = 2\pi(88 \pm 3)$ Hz is applied at the same time (green). (**B**) An example of measured mechanical fluctuations along the BAE pump axis (red circles) and the probe axis (blue circles). ϕ is the angle between these two axes. The blue line is a fit to $A\sin^2\phi + B$ (*21*). (**C**) Polar plot of (B), defining X_1 and X_2 along the direction of minimum and maximum fluctuation, respectively. (**D**) Mechanical fluctuations along the probe axis ($\langle X(\phi)^2\rangle$) at different microwave noise powers: Δη = 5.71, 9.17, 13.41, and 20.99 (±0.04) aW/Hz (brown, green, blue, and red dots, respectively). (**E**) Back-action in the X_2 quadrature normalized by quantum back-action $\langle X_2^2\rangle_{qba} = 2(\Gamma_{opt}/\Gamma_m)x_{zp}^2$. Inset, the microwave noise spectrum at microwave occupation factor $n_c \approx 0.9$. Δη is the noise density from the noise floor at ω_c, proportional to n_c. The sharp peak at the center is the mechanical sideband at $n_p = 1.3 \times 10^6$.

evading mechanism can be also understood by observing that X_1 and X_2 are constants of motion and thus quantum nondemolition observables (*12*).

The mechanical quadrature fluctuations are computed as

$$\langle X_1^2\rangle/x_{zp}^2 = 1 + 2n_m + 2n_{bad}$$
$$\langle X_2^2\rangle/x_{zp}^2 = 1 + 2n_m + 2n_{ba}^{BAE} + 2n_{bad} \quad (1)$$

where $n_{ba}^{BAE} = (\Gamma_{opt}/\Gamma_m)(2n_c + 1)$, $n_{bad} = [\kappa^2/(32\omega_m^2)]n_{ba}^{BAE}$, and Γ_m is the mechanical damping rate (*14*). One sees that the uncoupled X_2 quadrature experiences the measurement back-action n_{ba}^{BAE}, proportional to n_p, but the back-action onto X_1 is reduced by $[\kappa^2/(32\omega_m^2)]$, which is expected to be small (1.5×10^{-3}) in our experiment due to the sideband resolution realized in our device ($\kappa/\omega_m = 0.217 \pm 0.002$) .

We first study the quadrature-dependent back-action using two sets of BAE tones, denoted as "pump" and "probe" (Fig. 2). The pump tones ($n_p = 1.1 \times 10^6$) are set 20 dB stronger than the probe tones, and we control the relative phase (ϕ) between the beat tones of these two sets. This setup allows us to control the phase of the mechanical quadrature measured by the probe tones, relative to the strong pump tones. The resulting output spectrum of the probe tones measures $\langle X(\phi)^2\rangle = \langle X_1^2\rangle\cos^2\phi + \langle X_2^2\rangle\sin^2\phi$ (*21*).

Figure 2, B and C, compare the signals from the two sets of BAE tones. The fluctuations at $\phi = \pi/2$ along the X_2 quadrature show maximal increase in fluctuations due to back-action from the BAE pumps, and the minimum fluctuations at $\phi = 0$ agree with $\langle X_1^2\rangle$ measured by the pump tones, demonstrating the avoidance of the back-action from the noise in the detection microwave field. The back-action noise into X_2, $\langle X_2^2\rangle_{ba} = 2n_{ba}^{BAE}x_{zp}^2$, is expected to be proportional to $2n_c$+1 (Eq. 1), where the first term (n_c) represents classical microwave noise and the second term (+1) is from the quantum fluctuations of microwave field. In Fig. 2, D and E, we explore $\langle X_2^2\rangle_{ba}$ as a function of n_c by injecting microwave noise from room temperature into the device. In the measurement of quadrature-dependent back-action shown in Fig. 2D, we clearly observe an increase of back-action in X_2, $\langle X_2^2\rangle_{ba} = \langle X(\phi = \pi/2)^2\rangle - \langle X(\phi = 0)^2\rangle$, as n_c increases.

To determine n_c, we concurrently measure the noise power density above the amplifier noise floor at ω_c ($\Delta\eta$), which is linearly related to n_c, using a cryogenic microwave switch (*21*) (Fig. 2E, inset). Figure 2E shows the observed $\langle X_2^2\rangle_{ba}$ versus $\Delta\eta$. We see that the relationship is linear but does not extrapolate to zero back-action for zero classical microwave noise at $\Delta\eta = 0$: The mechanical device experiences a fluctuating force in excess of the classical noise contribution. The offset we observe is 1.1 ± 0.1, which is calibrated with high accuracy through the mechanical thermal calibration (*21*). This agrees well with the "+1" in n_{ba}^{BAE} expected from the quantum fluctuations in the microwave field, with a minor contribution of thermal $n_c \approx 0.1$ (*21*). In addition, the slope in the fit to Eq. 1 yields the calibration of classical microwave noise: $n_c/\Delta\eta = 0.22 \pm 0.02$ $(aW/Hz)^{-1}$. Most important, this measurement constitutes the first demonstration of mechanical detection of the quantum fluctuations of a microwave field (*23*, *24*).

The back-action from both the classical and quantum noise of the detection electromagnetic field is avoided in a single-quadrature measurement of motion with two-tone BAE. However, in general, the mechanical motion can also experience measurement back-action from sources other than the noise in the detection field. For instance, the increase in mechanical fluctuations due to thermal dissipation in the device is not avoided in BAE. To quantify these other back-action effects, and measure the total back-action into X_1, we measure the initial thermal motion and observe the increase in $\langle X_1^2\rangle$. We also measure $\langle x^2\rangle$ in a non-BAE configuration to compare the back-action (*21*). As expected, we observe that the BAE spectrum exhibits reduced back-action compared to the non-BAE case (Fig. 3, A and B). In Fig. 3C, we plot the initial thermal motion $\langle x^2\rangle_0$, $\langle x^2\rangle$ from non-BAE, and $\langle X_1^2\rangle$ from BAE at various pump strengths. In Fig. 3D, the total measurement back-action, $\langle x^2\rangle_{ba}$ and $\langle X_1^2\rangle_{ba}$, and the measurement imprecision, $\langle x^2\rangle_{imp}$ and $\langle X_1^2\rangle_{imp}$, are plotted. Here, we define n_p as $n_p = |a_{pump}^2|/2$ for BAE and $n_p = |a_{pump}^2|/4$ for non-BAE in order to compare the imprecision and back-action in these two pump configurations properly (*21*).

In non-BAE, as the imprecision decreases, the fluctuations due to back-action increase (blue dots in Fig. 3D). At $n_p = 2.3 \times 10^6$, the mechanical occupation increases from 13.0 ± 0.5 to 68.5 ±

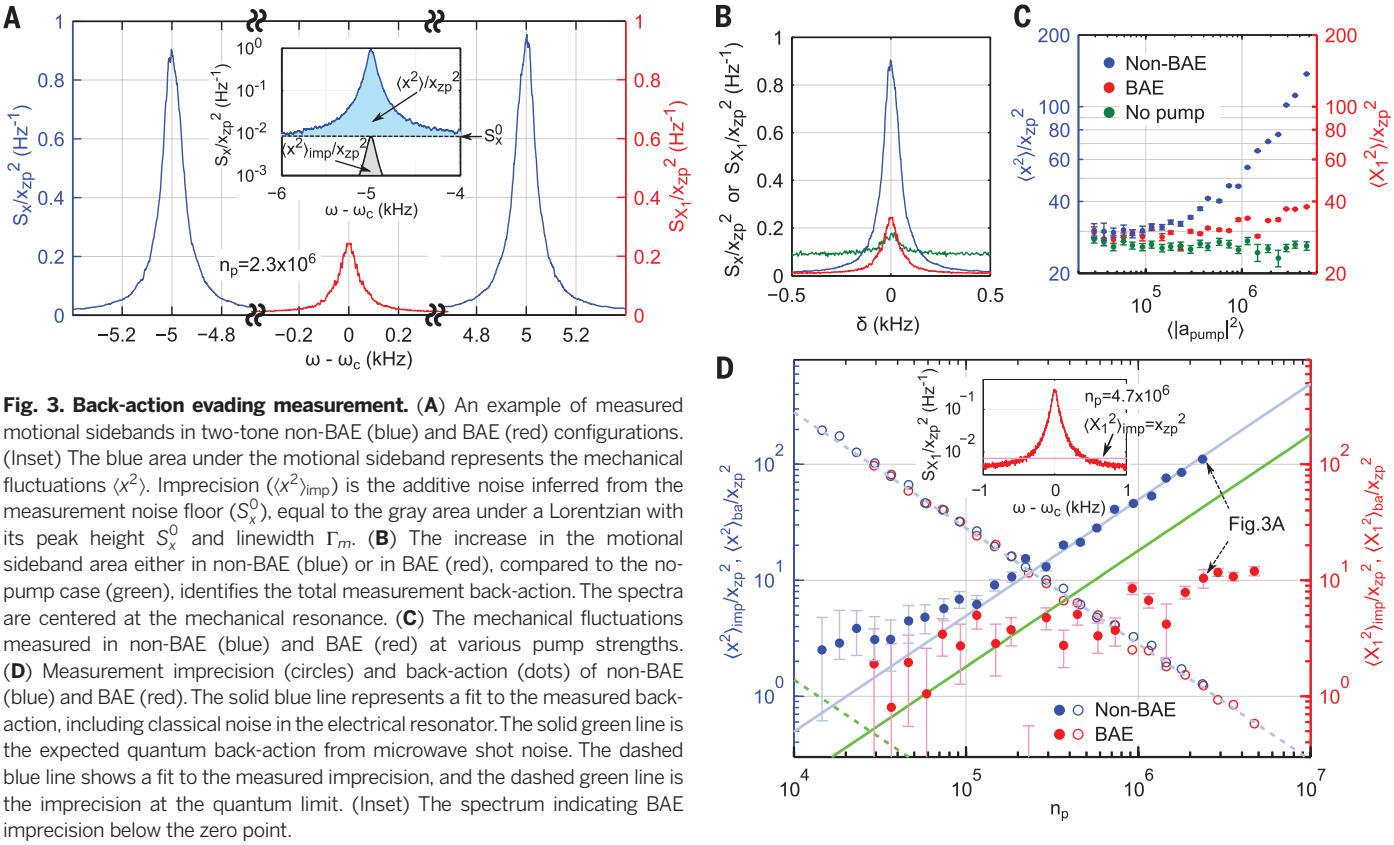

Fig. 3. Back-action evading measurement. (**A**) An example of measured motional sidebands in two-tone non-BAE (blue) and BAE (red) configurations. (Inset) The blue area under the motional sideband represents the mechanical fluctuations $\langle x^2\rangle$. Imprecision ($\langle x^2\rangle_{imp}$) is the additive noise inferred from the measurement noise floor (S_x^0), equal to the gray area under a Lorentzian with its peak height S_x^0 and linewidth Γ_m. (**B**) The increase in the motional sideband area either in non-BAE (blue) or in BAE (red), compared to the no-pump case (green), identifies the total measurement back-action. The spectra are centered at the mechanical resonance. (**C**) The mechanical fluctuations measured in non-BAE (blue) and BAE (red) at various pump strengths. (**D**) Measurement imprecision (circles) and back-action (dots) of non-BAE (blue) and BAE (red). The solid blue line represents a fit to the measured back-action, including classical noise in the electrical resonator. The solid green line is the expected quantum back-action from microwave shot noise. The dashed blue line shows a fit to the measured imprecision, and the dashed green line is the imprecision at the quantum limit. (Inset) The spectrum indicating BAE imprecision below the zero point.

0.1, consistent with a small finite microwave occupation factor ($n_c \approx 0.6 \pm 0.1$) in addition to the quantum fluctuations. In contrast, we do not observe a large increase in the mechanical fluctuations in BAE as the imprecision decreases (red dots in Fig. 3D). The expected back-action into the measured quadrature due to the finite sideband resolution (*14*) is $0.12x_{zp}^2$ at $n_p = 4.7 \times 10^6$. The measured back-action of $\langle X_1^2 \rangle_{ba} \approx 10x_{zp}^2$ is likely due to thermal dissipation in our device. Nonetheless, we demonstrate avoidance of the back-action noise by 10.7 ± 0.3 dB at $n_p = 2.3 \times 10^6$ compared with non-BAE. Most important, we show that the back-action $\langle X_1^2 \rangle_{ba}$ is 8.5 ± 0.4 dB below the level set by quantum fluctuations of the microwave field, $2(\Gamma_{opt}/\Gamma_m)x_{zp}^2$, at $n_p = 4.7 \times 10^6$.

In addition, the quadrature imprecision is below x_{zp}^2 at this point: $\langle X_1^2 \rangle_{imp} = (0.57 \pm 0.09)x_{zp}^2$ (Fig. 3D, inset). This is approximately a factor of 200 above that of quantum-limited imprecision, which is consistent with the detection efficiency determined by $\kappa_R/\kappa \approx 0.5$, the microwave loss between the device and amplifier (≈2 dB), and the noise temperature (≈4 K) of the amplifier at 4 K stage.

Quantum fluctuations of a single mode in a microwave field can be sensed with a mechanical system, and, with the proper pump field, these fluctuations can be steered into an unobserved aspect of the motion. These results lead the way toward measuring and manipulating the quantum noise of a mechanical resonator. As described in (*14*), feedback on the motion may be applied to produce a squeezed state from a thermal state. Using a nearly quantum-limited amplifier (*25*), we expect the generation of a squeezed state ($\langle X_1^2 \rangle / x_{zp}^2 < 1$) with $n_p \approx 10^5$, which would be useful for detection of weak forces and fundamental studies of quantum decoherence (*26*). Finally, we note that the mechanical mode reaching 7.2 mK demonstrates a new application of a micromechanical resonator as a primary ultralow-temperature thermometer.

REFERENCES AND NOTES

1. R. W. P. Drever, J. Hough, W. A. Edelstein, J. R. Pugh, W. Martin, *Proc. Int. Mtg on Experimental Gravitation, Pavia, Italy*, B. Bertotti, Ed. (Accademia Nazionale Dei Lincei, Rome, 1976).
2. C. M. Caves, K. S. Thorne, R. W. P. Drever, V. D. Sandberg, M. Zimmermann, *Rev. Mod. Phys.* **52**, 341–392 (1980).
3. J. D. Teufel, T. Donner, M. A. Castellanos-Beltran, J. W. Harlow, K. W. Lehnert, *Nat. Nanotechnol.* **4**, 820–823 (2009).
4. G. Anetsberger *et al.*, *Phys. Rev. A* **82**, 061804 (2010).
5. S. Schreppler *et al.*, Optically measuring force near the standard quantum limit. arXiv:1312.4896 (2013).
6. A. Naik *et al.*, *Nature* **443**, 193–196 (2006).
7. K. W. Murch, K. L. Moore, S. Gupta, D. M. Stamper-Kurn, *Nat. Phys.* **4**, 561–564 (2008).
8. T. P. Purdy, R. W. Peterson, C. A. Regal, *Science* **339**, 801–804 (2013).
9. V. B. Braginsky, F. Y. Khalili, *Quantum Measurement* (Cambridge Univ. Press, Cambridge, 1992).
10. R. Ruskov, K. Schwab, A. N. Korotkov, *Phys. Rev. B* **71**, 235407 (2005).
11. V. B. Braginsky, Y. I. Vorontsov, *Sov. Phys. Usp.* **17**, 644–650 (1975).
12. K. S. Thorne, R. W. P. Drever, C. M. Caves, M. Zimmermann, V. D. Sandberg, *Phys. Rev. Lett.* **40**, 667–671 (1978).
13. V. B. Braginsky, Y. I. Vorontsov, K. S. Thorne, *Science* **209**, 547–557 (1980).
14. A. A. Clerk, F. Marquardt, K. Jacobs, *New J. Phys.* **10**, 095010 (2008).
15. J. D. Teufel *et al.*, *Nature* **475**, 359–363 (2011).
16. J. Suh, M. D. Shaw, H. G. Leduc, A. J. Weinstein, K. C. Schwab, *Nano Lett.* **12**, 6260–6265 (2012).
17. J. Suh, A. J. Weinstein, K. C. Schwab, *Appl. Phys. Lett.* **103**, 052604 (2013).
18. M. F. Bocko, R. Onofrio, *Rev. Mod. Phys.* **68**, 755–799 (1996).
19. F. Marquardt, J. P. Chen, A. A. Clerk, S. M. Girvin, *Phys. Rev. Lett.* **99**, 093902 (2007).
20. J. B. Hertzberg *et al.*, *Nat. Phys.* **6**, 213–217 (2010).
21. Materials and methods are available as supplementary materials on *Science* Online.
22. T. Rocheleau *et al.*, *Nature* **463**, 72–75 (2010).
23. R. H. Koch, D. J. Van Harlingen, J. Clarke, *Phys. Rev. B* **26**, 74–87 (1982).
24. A. Fragner *et al.*, *Science* **322**, 1357–1360 (2008).
25. J. Y. Mutus *et al.*, *Appl. Phys. Lett.* **103**, 122602 (2013).
26. B. L. Hu, Y. Zhang, *Mod. Phys. Lett. A* **8**, 3575–3584 (1993).

ACKNOWLEDGMENTS

We would like to acknowledge J. Hertzberg, T. Rocheleau, T. Ndukum, and M. Shaw for work on earlier experiments that led to these results. This work is supported by funding provided by the Institute for Quantum Information and Matter, an NSF Physics Frontiers Center with support of the Gordon and Betty Moore Foundation (NSF-IQIM 1125565), by the Defense Advanced Research Projects Agency (DARPA-QUANTUM HR0011-10-1-0066), and by NSF (NSF-DMR 1052647 and NSF-EEC 0832819).

SUPPLEMENTARY MATERIALS

www.sciencemag.org/content/344/6189/1262/suppl/DC1
Materials and Methods
Figs. S1 to S4
References (*27*–*31*)

12 March 2014; accepted 2 May 2014
Published online 15 May 2014;
10.1126/science.1253258

EARTH'S INTERIOR

Dehydration melting at the top of the lower mantle

Brandon Schmandt,[1]* Steven D. Jacobsen,[2]* Thorsten W. Becker,[3] Zhenxian Liu,[4] Kenneth G. Dueker[5]

The high water storage capacity of minerals in Earth's mantle transition zone (410- to 660-kilometer depth) implies the possibility of a deep H_2O reservoir, which could cause dehydration melting of vertically flowing mantle. We examined the effects of downwelling from the transition zone into the lower mantle with high-pressure laboratory experiments, numerical modeling, and seismic *P*-to-*S* conversions recorded by a dense seismic array in North America. In experiments, the transition of hydrous ringwoodite to perovskite and (Mg,Fe)O produces intergranular melt. Detections of abrupt decreases in seismic velocity where downwelling mantle is inferred are consistent with partial melt below 660 kilometers. These results suggest hydration of a large region of the transition zone and that dehydration melting may act to trap H_2O in the transition zone.

The water content of the upper mantle as sampled by mid-ocean ridge basalts is 0.005 to 0.02 weight % (wt %) (*1*), but a potentially much larger, deep reservoir of water may exist in the mantle transition zone between 410- and 660-km depth owing to the 1 to 3 wt % H_2O storage capacity of the major mineral phases wadsleyite and ringwoodite (*2*, *3*). Convective mass transfer across the boundaries of the transition zone could cause dehydration melting, and consequently filtering of incompatible elements, if water contents in the transition zone exceed that of the shallower or deeper mantle (*4*). An open question is whether transition zone water contents are sufficient to cause dehydration melting where there is downward flow into the lower mantle.

[1]Department of Earth and Planetary Science, University of New Mexico, Albuquerque, NM, USA. [2]Department of Earth and Planetary Sciences, Northwestern University, Evanston, IL, USA. [3]Department of Earth Sciences, University of Southern California, Los Angeles, CA, USA. [4]Geophysical Laboratory, Carnegie Institution of Washington, Washington DC, USA. [5]Department of Geology and Geophysics, University of Wyoming, Laramie, WY, USA.
***Corresponding author. E-mail: bschmandt@unm.edu (B.S.); steven@earth.northwestern.edu (S.D.J.)**

Dehydration melting due to downward flow across the 660-km discontinuity (660) would require both hydration of ringwoodite in the transition zone and low water storage capacity at the top of the lower mantle. The recent discovery of a ~1.5 wt % H_2O hydrous ringwoodite inclusion in a diamond (*5*) demonstrates that, at least locally, the mantle transition zone may be close to water saturation. Regional detections of high seismic attenuation (*6*) and electrical conductivity (*7*) in the transition zone suggest hydration at larger scales. However, high-pressure experiments on the incorporation of H_2O into silicate perovskite vary widely from 0.0001 wt % (*8*) to 0.4 wt % H_2O (*9*), with other estimates in between (*10*). Recent experiments on coexisting phase assemblages indicate a high H_2O partition coefficient between ringwoodite and silicate perovskite of 15:1 (*11*), suggesting a large contrast in water storage capacity at the boundary between the base of the transition zone and the top of the lower mantle.

We integrated laboratory experiments, seismic imaging, and numerical models of mantle flow to investigate mass transfer and melting at the interface between the transition zone and lower mantle beneath North America (*12*). We conducted in situ

Editor's Summary

Avoiding back-action in quantum measurements

The very process of measuring a quantum system has an influence on the system through the process of back-action. Suh *et al.* used a back-action evasion scheme to monitor the motion of a miniature oscillator without influencing its motion (see the Perspective by Bouwmeester). The scheme should help in the understanding of the fundamental limits associated with measurement and will have practical implications in providing a low-temperature thermometer and a probe of extremely weak forces.

Science, this issue p. 1262